Analytical Sensitivity of Locational Customer Directrix Load to Line Capacity for Quantifying Demand Response Contribution to Congestion Mitigation

Yan Meng[†,1], Shuyang Shen[†,1], Lei Yan[*,1], Jiayu Han[2], Guofeng Wang[2], Yi Zhang[3], Yongzhi Zhou[1], Zuyi Li[1], *Fellow, IEEE*
[1]*College of Electrical Engineering, Zhejiang University,* Hangzhou, China
[2]*College of Information Engineering, Zhejiang University of Technology*, Hangzhou, China
[3]*School of Electrical Engineering, Shanghai Jiao Tong University*, Shanghai, China

***Abstract*—Recent studies have proposed customer directrix load (CDL)-based demand response (DR) as a scalable scheme for dispatching load flexibility. However, they lack an explicit analysis of how network constraints shape CDL formation and thus cannot quantify DR contributions at different locations to mitigating congestion. This paper embeds network constraints into DR target design and explicitly characterizes the mapping relationship between variations in line capacity limits and locational CDL (LCDL), which serves as a spatially specific guiding target curve for participants. Based on the LCDL formulation, we rigorously derive the analytical sensitivity of LCDL with respect to line capacity, revealing the incremental change in LCDL induced by a unit change in line capacity. This mathematical result turns black-box CDL outcomes into explainable signals for DR participants. Furthermore, we demonstrate that this sensitivity serves as a marginal contribution indicator of the DR target at each location and time interval to congestion mitigation on a specific line. Comprehensive case studies verify the theoretical derivation, demonstrating LCDL's superiority over conventional CDL in renewable energy accommodation and its scalability for larger power networks.**

***Index Terms*—Demand response, customer directrix load, network constraint, sensitivity analysis, congestion mitigation.**

I. Introduction

The mushrooming of distributed energy resources (DERs) positions demand response (DR) as a promising means of providing flexibility to the power gird[1][2]. The International Energy Agency has called for large-scale DR deployment to alleviate the burden of power balancing[3]. However, as the number of DR participants increases, the incompatibilities of the current DR schemes with large-scale DR deployment have been highlighted and the insufficient consideration of network constraints in large-scale DR has become increasingly prominent.

The two mainstream types of current DR schemes include incentive-based DR and price-based DR [4]. For incentive-based DR scheme, calculation of customer baseline load (CBL) faces several obstacles under large-scale DR, such as heavy computational burden, "moral hazard" problem, and lack of simplicity, etc [5]. In addition, the inherent limitations of time-varying prices impede the large-scale deployment of price-based DR, including overshoot, lack of straightforward guiding targets for customers, and hard to accurately and dynamically reflect the adjustment demands of power systems [6].

Customer directrix load (CDL)-based DR is a novel scheme proposed in [6] which is compatible with the large-scale deployment of DR for its simplicity, goal-directedness, and fairness. CDL characterizes what profile of load curve is beneficial to system power balance, and customers are guided to adjust their consumption toward this profile. The higher the similarity between a customer's post-DR load curve and CDL, the greater the financial incentive received. The problems of CBL and time-varying prices can be promisingly overcome since they are omitted under CDL-based DR. An optimization model of customer power consumption was developed to consider their comfort and preference under CDL-based DR [7]. In [8], the load and renewable energy (RE) uncertainties were embedded into the CDL formulation.

With the proliferation of RE and DERs in different locations of power systems, the discrepancies of RE accommodation demands in different locations becomes prominent and the resulting line congestions are exacerbated. Besides, network constraints have a non-negligible impact on the delivery of the flexibility of DR customers in different locations [9], especially in large-scale DR. In other words, the contribution performance of DR customers is to some extent affected by network constraints [10]. A transmission-distribution coordinated DR mechanism that adopts locational CDL (LCDL) as the guiding target for participants at each node was proposed in [11]. *Although network constraints are incorporated, how they influence LCDL has not been analyzed and the LCDL formation mechanism remains unclear.* This lack of explanation for why DR target curves differ across nodes may reduce participants' acceptance of LCDL and their willingness to participate in DR. Moreover, *how to quantify the contributions of DR targets at different nodes to mitigating line congestion remains unaddressed*, which is crucial for facilitating high-penetration RE accommodation in heavily congested power systems.

To bridge the gaps, this paper elucidates the formation mechanism of LCDL under network constraints by establishing the mapping between line capacity variations and the resulting LCDL change, and, on this basis, a quantitative metric is proposed to quantify the contributions of locational DR targets to congestion mitigation. It possessed two salient features:

(1) Construct the mapping between variations in line capacity limits and variations in LCDL: The analytical sensitivity of LCDL to line capacity is rigorously derived, revealing the incremental change in LCDL induced by a unit change in line capacity. This sensitivity turns black-box CDL outcomes into explainable signals for DR participants.

(2) Propose a quantitative metric for contributions of

†: *contribute equally to this work* *: *corresponding author*

This work was supported by National Natural Science Foundation of China (52307147) and Zhejiang Province College Students' Science and Technology Innovation Activity Plan (2025R401154).

979-8-3315-8138-1

locational DR targets to line congestion mitigation: It is proved that the sensitivity of LCDL with respect to line capacity serves as a marginal contribution indicator of the DR target at each location and time interval to congestion mitigation on a specific line. Based on this, a quantitative metric for contribution assessment is presented.

II. Methodology

A. Concept of LCDL

Under large-scale DR, customers make non-negligible contributions to power balancing. System resources can be classified into adjustable and non-adjustable. Adjustable resources include conventional units and flexible loads, while non-adjustable resources comprise inelastic loads and RE output. Variations induced by non-adjustable resources must be offset by adjustable ones. LCDL represents an optimally designed guiding target by the system operator rather than a behavioral prediction, characterizing the load profile most beneficial to system power balance and congestion mitigation. Guided by LCDL, customers reshape their load curves by shifting consumption without changing the total energy, and receive incentives according to how well their profiles match the LCDL. Fig. 1 depicts the schematic diagram of LCDL. When DR is activated, the system operator (SO) first calculates the power variation that needs to be mitigated based on the RE maximal output and power consumption of non-DR customers. Then, the SO formulates LCDLs and release them to enrolled DR customers in the pertinent location. Notably, the spatial discrepancies of the power adjustment demand deriving from the non-adjustable resources in different locations are reflected in the discrepancies of LCDLs.

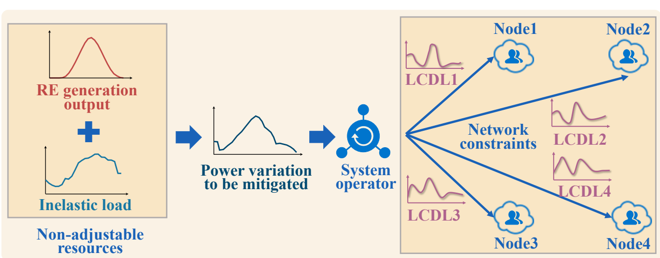

Fig. 1 Schematic diagram of LCDL.

B. Formulation of LCDL

The profile of a power or load vector $\boldsymbol{p}=[p_1,p_2,\dots,p_T]^{\mathrm{T}}$ is defined as: $prf(\boldsymbol{p})=\boldsymbol{p}/(\boldsymbol{p}^{\mathrm{T}}\cdot\mathbf{1})$. When network constraints are neglected, the equality of the adjustable balancing non-adjustable is shown in (1):

$$\sum_{g\in\mathcal{G}} E_{\mathrm{G},g}\boldsymbol{RRC}-\sum_{d\in\mathcal{D}} E_{\mathrm{D},d}\boldsymbol{CDL}=\sum_{i\in\mathcal{I}}\boldsymbol{P}_{\mathrm{I},i}-\sum_{r\in\mathcal{R}}\boldsymbol{P}_{\mathrm{R},r}^{\max} \tag{1}$$

where g, d, i, r are the indexes of conventional units, DR customers, inelastic loads, and RE plants, respectively, with the corresponding sets being $\mathcal{G}$, $\mathcal{D}$, $\mathcal{I}$, and $\mathcal{R}$. $E_{\mathrm{G},g}$ and $E_{\mathrm{D},d}$ denote the total energy of each conventional unit and flexible load, respectively. $\boldsymbol{RRC}$ is the system-level adjustment demand curve vector of conventional units. $\boldsymbol{CDL}$ is the system-level CDL vector of DR customers. $\boldsymbol{P}_{\mathrm{I},i}$ is the power vector of inelastic loads. $\boldsymbol{P}_{\mathrm{R},r}^{\max}$ denotes the maximal output of RE.

Under CDL-based DR scheme, conventional units and DR customers, as the adjustable resources, bear the same power adjustment responsibility. Due to the inherent differences of power generation and consumption between conventional units and DR customers, $\boldsymbol{RRC}$ and $\boldsymbol{CDL}$ take on opposite profiles, as shown in (2).

$$\boldsymbol{RRC}+\boldsymbol{CDL}=\frac{2}{T}\cdot\mathbf{1}\quad t\in\mathcal{T} \tag{2}$$

where t is the index of time slot with its set $\mathcal{T}=\{1,2,\dots,T\}$. The system-level CDL in Eq. (3) is derived by integrating global balance requirements from Eq. (1) with the shared responsibility principle in Eq. (2):

$$\boldsymbol{CDL}=\frac{2\sum_{g\in\mathcal{G}}E_{\mathrm{G},g}+T\left(\sum_{r\in\mathcal{R}}\boldsymbol{P}_{\mathrm{R},r}^{\max}-\sum_{i\in\mathcal{I}}\boldsymbol{P}_{\mathrm{I},i}\right)}{T\left(\sum_{g\in\mathcal{G}}E_{\mathrm{G},g}+\sum_{d\in\mathcal{D}}E_{\mathrm{D},d}\right)} \tag{3}$$

Notably, the system-level CDL characterizes the adjustment demand on the time scale and serves as the unified guiding target for all DR customers regardless of system network constraints. We define the system-level CDL as the unified CDL (UCDL) which will be further compared with LCDLs in Section 3. In practice, the adjustment demand of different locations varies since the non-adjustable resources are distributed in different locations. Therefore, LCDLs are further developed to characterize the adjustment demand of different locations under network constraints, shown as problem $\boldsymbol{\Phi}$. The objective function is to minimize the sum of squares of LCDL variations relative to the system-level CDL, as shown in (4). Constraint (5) denotes that the total energy of each DR customer remains unchanged. (6) is the profile constraint to the characteristic of customers consuming power. (7) guarantees the power balance in each period. (8) represents the line capacity constraints.

$$\boldsymbol{\Phi}:\min_{\Delta_{CDL,d,t}}\ \sum_{d\in\mathcal{D}}\sum_{t\in\mathcal{T}}\Delta_{CDL,d,t}^2 \tag{4}$$

s.t.

$$\sum_{t\in\mathcal{T}}\Delta_{CDL,d,t}=0\quad d\in\mathcal{D} \tag{5}$$

$$0\le CDL_t+\Delta_{CDL,d,t}\le 1\quad d\in\mathcal{D},t\in\mathcal{T} \tag{6}$$

$$\sum_{d\in\mathcal{D}}E_{\mathrm{D},d}\Delta_{CDL,d,t}=0\quad t\in\mathcal{T} \tag{7}$$

$$\begin{aligned}P_{\mathrm{L},l}^{\min}\le\sum_{g\in\mathcal{G}}H_{g-l}P_{g,t}+\sum_{r\in\mathcal{R}}H_{r-l}P_{\mathrm{R},r,t}^{\max}-\sum_{i\in\mathcal{I}}H_{i-l}P_{\mathrm{I},i,t}\\-\sum_{d\in\mathcal{D}}H_{d-l}E_{\mathrm{D},d}(CDL_t+\Delta_{CDL,d,t})\le P_{\mathrm{L},l}^{\max}\quad l\in\mathcal{L},t\in\mathcal{T}\end{aligned} \tag{8}$$

where $\Delta_{CDL,d,t}$ denote the variations LCDL with respect to $\boldsymbol{CDL}$, respectively. l is the index of lines with its set $\mathcal{L}$. $P_{\mathrm{L},l}^{\min}$ and $P_{\mathrm{L},l}^{\max}$ denote the line flow limits. $H_{g-l},H_{d-l},H_{r-l},H_{i-l}$ are the power transfer distribution factor of conventional unit g, DR customer d, RE generation r, inelastic load i on line l, respectively. Let $\tilde{\Delta}_{CDL,d,t}$ denotes the optimum of problem $\boldsymbol{\Phi}$. Therefore, LCDLs can be obtained in (9).

$$LCDL_{d,t}=CDL_t+\tilde{\Delta}_{CDL,d,t}\quad d\in\mathcal{D},t\in\mathcal{T} \tag{9}$$

It should be noted that while the locational components of LCDL are mathematically analogous to the congestion component of LMP, LCDL provides direct guiding targets whereas LMP functions as indirect price signal. Unlike price-based DR, where signals such as TOU or RTP derived from LMPs often trigger rebound effects or peak valley inversion, the proposed LCDL targets provide explicit profiles that ensure stable load adjustments. Besides, this LCDL-based DR framework is adaptable to diverse objectives such as RE accommodation and carbon reduction, offering greater versatility than conventional

979-8-3315-8138-1

congestion management signals.

C. Analytical Sensitivity of LCDL to Line Capacity

We transform the problem $\boldsymbol{\Phi}$ into the following compact matrix form:

$$\min \quad \boldsymbol{\Delta}^T\boldsymbol{\Delta} \tag{10}$$

$$\text{s.t.} \quad \boldsymbol{A}\boldsymbol{\Delta} = \boldsymbol{b} : \boldsymbol{\pi} \tag{11}$$

$$\boldsymbol{B}\boldsymbol{\Delta} \geq \boldsymbol{v}(\boldsymbol{P}_{\mathrm{L}}^{\max}) : \boldsymbol{\alpha} \tag{12}$$

$$\boldsymbol{B}\boldsymbol{\Delta} \leq \boldsymbol{u}(\boldsymbol{P}_{\mathrm{L}}^{\max}) : \boldsymbol{\beta} \tag{13}$$

where $\boldsymbol{\Delta} = [\boldsymbol{\Delta}_{CDL,1}^T, \boldsymbol{\Delta}_{CDL,2}^T \cdots \boldsymbol{\Delta}_{CDL,T}^T]^T$ denotes the decision variables, in which $\boldsymbol{\Delta}_{CDL,d}^T = [\Delta_{CDL,d,1}, \Delta_{CDL,d,2} \cdots \Delta_{CDL,D,T}]^T$, where d is the index of flexible load with its set $\mathcal{D} = \{1,2,\ldots,D\}$. Dual variables $\boldsymbol{\pi}$, $\boldsymbol{\alpha}$, $\boldsymbol{\beta}$ represent objective function sensitivity to constraint relaxation. While $\boldsymbol{\pi}$ reflects energy balance impacts, $\boldsymbol{\alpha}$ and $\boldsymbol{\beta}$ serve as congestion indicators where non zero values identify bottlenecks shaping locational DR targets.

$\boldsymbol{A}\boldsymbol{\Delta} = \boldsymbol{b}$ denotes the equality constraints (5) and (7) in the original problem $\boldsymbol{\Phi}$:

$$\boldsymbol{A} = \begin{bmatrix} \mathbf{1}_{1\times T} & \mathbf{0}_{1\times T} & \cdots & \mathbf{0}_{1\times T} \\ \mathbf{0}_{1\times t} & \mathbf{1}_{1\times T} & \cdots & \mathbf{0}_{1\times T} \\ \cdots & \cdots & \cdots & \mathbf{0}_{1\times T} \\ \mathbf{0}_{1\times T} & \mathbf{0}_{1\times T} & \mathbf{0}_{1\times T} & \mathbf{1}_{1\times T} \\ E_{D,1}\boldsymbol{E}_{T\times T} & E_{D,2}\boldsymbol{E}_{T\times T} & \cdots & E_{D,d}\boldsymbol{E}_{T\times T} \end{bmatrix} \tag{14}$$

$$\boldsymbol{b} = \mathbf{0}_{(T+D)\times 1} \tag{15}$$

where index $i \times j$ means the matrix has i rows and j columns. $\mathbf{1}$ is the unit matrix, $\mathbf{1}$ is the zero matrix, $\boldsymbol{E}$ is the identity matrix. The first $D \times T$ rows are the constraints (5) and the last T rows are the constraints (7) in the original problem $\boldsymbol{\Phi}$.

$\boldsymbol{v}(\boldsymbol{P}_{\mathrm{L}}^{\max}) \leq \boldsymbol{B}\boldsymbol{\Delta} \leq \boldsymbol{u}(\boldsymbol{P}_{\mathrm{L}}^{\max})$ denotes the inequality constraints (6) and (8) in the original problem $\boldsymbol{\Phi}$:

$$\boldsymbol{B} = [(-\boldsymbol{HQB}_1)^T, \boldsymbol{E}_{DT\times DT}]^T \tag{16}$$

$$\boldsymbol{v}(\boldsymbol{P}_{\mathrm{L}}^{\max}) = [(-\boldsymbol{P}_{\mathrm{L}}^{\max} - \boldsymbol{HP}_1^{inj})^T \ldots (-\boldsymbol{P}_{\mathrm{L}}^{\max} - \boldsymbol{HP}_T^{inj})^T, -\boldsymbol{CDL}^T \ldots]^T \tag{17}$$

$$\boldsymbol{u}(\boldsymbol{P}_{\mathrm{L}}^{\max}) = [(\boldsymbol{P}_{\mathrm{L}}^{\max} - \boldsymbol{HP}_1^{inj})^T \ldots (\boldsymbol{P}_{\mathrm{L}}^{\max} - \boldsymbol{HP}_T^{inj})^T, (\mathbf{1} - \boldsymbol{CDL})^T \ldots]^T \tag{18}$$

where $\boldsymbol{D}(\cdot)$ converts the vector into a diagonal matrix, $\boldsymbol{Q}$ is a diagonal matrix, equals to $\boldsymbol{D}([E_{D,1}, E_{D,2}, \cdots E_{D,D}])$. $\boldsymbol{B}_1$ is an elementary row transformation matrix satisfying:

$$\begin{cases} \boldsymbol{B}_1\boldsymbol{\Delta}_{CDL}^T = \boldsymbol{\Lambda}_{CDL}^T = [\boldsymbol{\Lambda}_{CDL,1}^T, \boldsymbol{\Lambda}_{CDL,2}^T \cdots \boldsymbol{\Lambda}_{CDL,T}^T]^T \\ \boldsymbol{\Lambda}_{CDL,t}^T = [\Delta_{CDL,1,t}, \Delta_{CDL,2,t} \cdots \Delta_{CDL,D,T}]^T \end{cases} \tag{19}$$

$\boldsymbol{P}_t^{inj}$ is the nodal injection of the system, forming the network constraints (5):

$$\boldsymbol{P}_t^{inj} = \boldsymbol{C}_g\boldsymbol{P}_{G,g,t} + \boldsymbol{C}_r\boldsymbol{P}_{R,r,t} - \boldsymbol{C}_l\boldsymbol{CDL} - \boldsymbol{C}_i\boldsymbol{P}_{I,i,t} \tag{20}$$

where $\boldsymbol{C}_r$, $\boldsymbol{C}_l$, $\boldsymbol{C}_i$ denote the inject position of the renewable energy unit, flexible load and inflexible load, respectively.

Thus, the Karush–Kuhn–Tucker (KKT) conditions can be obtained:

$$\begin{cases} \boldsymbol{A}\boldsymbol{\Delta} = \boldsymbol{b} \\ \boldsymbol{B}\boldsymbol{\Delta} + \boldsymbol{w}_1 = \boldsymbol{u} \\ \boldsymbol{v} + \boldsymbol{w}_2 = \boldsymbol{B}\boldsymbol{\Delta} \\ \boldsymbol{w}_1, \boldsymbol{w}_2, \boldsymbol{\alpha}, \boldsymbol{\beta} \geq \mathbf{0} \\ \boldsymbol{D}(\boldsymbol{w}_1)\boldsymbol{\beta} = \mathbf{0} \\ \boldsymbol{D}(\boldsymbol{w}_2)\boldsymbol{\alpha} = \mathbf{0} \\ \boldsymbol{A}^T\boldsymbol{\pi} - \boldsymbol{B}^T\boldsymbol{\beta} + \boldsymbol{B}^T\boldsymbol{\alpha} = 2\boldsymbol{\Delta} \end{cases} \tag{21}$$

where $\boldsymbol{w}_1$, $\boldsymbol{w}_2$, are the slack variables. Substituting the slack variables into the complementary slackness conditions and take the derivative of the KKT condition respect to the flow limit, we have $\boldsymbol{N} \cdot \boldsymbol{S} = \boldsymbol{f}$:

$$\begin{bmatrix} \mathbf{0} & \boldsymbol{A} & \mathbf{0} & \mathbf{0} \\ \boldsymbol{A}^T & 2\boldsymbol{E} & \boldsymbol{B}^T & \boldsymbol{B} \\ \mathbf{0} & \boldsymbol{D}(\boldsymbol{\beta})\boldsymbol{B} & -\boldsymbol{D}(\boldsymbol{w}_1) & \mathbf{0} \\ \mathbf{0} & \boldsymbol{D}(\boldsymbol{\alpha})\boldsymbol{B} & \mathbf{0} & \boldsymbol{D}(\boldsymbol{w}_2) \end{bmatrix} \begin{bmatrix} \dfrac{\partial \boldsymbol{\pi}}{\partial \boldsymbol{P}_{\mathrm{L}}^{\max}} \\ \dfrac{\partial \boldsymbol{\Delta}_{CDL}}{\partial \boldsymbol{P}_{\mathrm{L}}^{\max}} \\ \dfrac{\partial \boldsymbol{\alpha}}{\partial \boldsymbol{P}_{\mathrm{L}}^{\max}} \\ \dfrac{\partial \boldsymbol{\beta}}{\partial \boldsymbol{P}_{\mathrm{L}}^{\max}} \end{bmatrix} = \begin{bmatrix} \mathbf{0} \\ \mathbf{0} \\ \boldsymbol{D}(\boldsymbol{\beta})\dfrac{\partial \boldsymbol{u}}{\partial \boldsymbol{P}_{\mathrm{L}}^{\max}} \\ \boldsymbol{D}(\boldsymbol{\alpha})\dfrac{\partial \boldsymbol{v}}{\partial \boldsymbol{P}_{\mathrm{L}}^{\max}} \end{bmatrix} \tag{22}$$

The second item $\boldsymbol{S}$ is the sensitivity of LCDL to network constraints, which can be obtained by (23). As noted in [12], $\boldsymbol{N}$ is typically invertible in most practical scenarios. However, under specific numerical conditions, $\boldsymbol{N}$ may undergo degeneracy and thus become singular. The pseudo-inverse formulation in (23) is specifically employed to ensure numerical stability and tractability in these degenerate cases.

$$\boldsymbol{S} = \frac{\partial \boldsymbol{\Delta}_{CDL}}{\partial \boldsymbol{P}_{\mathrm{L}}^{\max}} = [\mathbf{0}, \boldsymbol{E}, \mathbf{0}, \mathbf{0}]\boldsymbol{N}^T(\boldsymbol{N}\boldsymbol{N}^T)^{-1}\boldsymbol{f} \tag{23}$$

D. Quantifying Contributions to congestion mitigation

Equations (24)-(27) establish metrics to quantify how nodal load adjustments mitigate network congestion. As we obtain the $\Delta_{CDL,d,t}$ and $\boldsymbol{S}$, for any $\Delta_{CDL,d,t}$, its impact to line l is:

$$\Delta_{l-d} = H_{l-d}\Delta_{CDL,d,t} \tag{24}$$

Eq. (24) calculates the specific power flow variation Δ_{l-d} on a congested line induced by the load adjustment at node d. Eq. (25) identifies congestion intervals and locations by extracting dual multipliers from network constraints:

$$\begin{cases} \breve{\mu}_{l,t} = \alpha_{L(t-1)+l} \\ \hat{\mu}_{l,t} = \beta_{L(t-1)+l} \end{cases} \tag{25}$$

Eq. (26) defines the total contribution by aggregating impacts across congested periods using the Kronecker Delta for directional distinction:

$$TC_d = \sum_t \delta_{\breve{\mu}_{l,t}} H_{l-d}\Delta_{CDL,d,t} - \delta_{\hat{\mu}_{l,t}} H_{l-d}\Delta_{CDL,d,t} \tag{26}$$

where $\delta_{i,j}$ is the Kronecker Delta. If $\delta_{\hat{\mu}_1,0} = 1$, the line is congestion on the forward directions, and if $\delta_{\mu_1,0} = 1$, the line is congestion on the reverse directions.

Eq. (27) defines the marginal contribution as the incremental flow reduction achieved by a unit change in the target, derived from sensitivity $\boldsymbol{S}$:

$$MC_d = -\sum_l H_{l-d} \sum_{i=(d-1)T}^{dT} S_{i,l} \tag{27}$$

Thus, by formulating the total and marginal index, specific motivation can be exerted to motivate customers with higher contribution.

III. Numerical Tests

A. Simulation Setup

A 3-bus system is initially employed to facilitate a clear analysis of LCDL formation mechanism and elucidate how network constraints influence LCDL. Depicted in Fig. 2(a), it features three load nodes with DR customer load proportion being 0.3, 0.4, and 0.3, respectively. Solar and wind plants are located at nodes 2 and 3. To focus on network impacts, conventional units are omitted and inelastic loads remain constant. The inelastic load curve and maximal output of RE are shown in Fig. 2(b). Four scenarios define line capacities [$x1$, $x2$, $x3$] for lines 1-2, 1-3, and 2-3 respectively: Case 1 [8,8,8] with full connectivity, while Cases 2 [0,8,8], 3 [8,0,8], and 4 [8,8,0] represent specific link disconnections. Based on these configurations, Section III.B analyzes the impact of network constraints on LCDL, while Section III.C evaluates RE accommodation performance.

To evaluate scalability, a modified IEEE 30 bus system with 41 branches and 20 load nodes is further examined in Section III.D. This system includes 6 thermal, 4 wind, and 6 PV units, while flexible loads constitute 50% of the nodal demand.

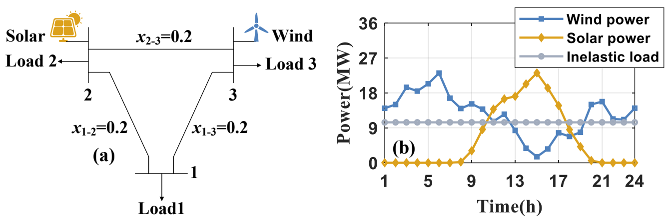

Fig. 2 3-bus system. (a) Topology. (b) Output of non-adjustable resources.

B. *Impacts of Network Constraints on LCDLs*

The LCDLs and power flow of each line in case 1-4 are depicted in Fig. 3-Fig. 6, respectively. It can be seen that LCDLs share the same profile as UCDL when there is no congestion. Obviously, UCDL is consistent with the profile of the sum of wind and solar output, which characterizes the system-level adjustment demand. When flow limits are binding, the LCDL of a node resembles the profile of its local or adjacent RE output.

In the cases 1-4, effectiveness of the sensitivity is verified by slacking 0.2MW on the capacity limit of line 2-3 for cases 1-3 and line 1-2 for case 4 and comparing the normalized value of the original LCDL (depict by solid line in (a)) and the slacked LCDL (depict by dashed line in (a)). No congestion is occurred in case 1, so the sensitivity matrix is all 0, and the solid and dashed line in Fig.3(a) overlap. In case 2, the sensitivity $S_{1,1,2-3} = -0.0025$, the original $LCDL_{1,1} = 0.03227$, the slacked $LCDL^s_{1,1} = 0.03177$ in which $0.03177 \approx 0.03227 - 0.0005$ satisfies $LCDL^s_{1,1} \approx LCDL_{1,1} + 0.2S_{1,1,2-3}$ very well. In case 3, sensitivity is bigger than case 1, $S_{1,4,2-3} = 0.025$, $LCDL_{1,4} = 0.0229$, $LCDL^s_{1,1} = 0.0279$, also satisfying $0.0279 \approx 0.0229 + 0.2 \times 0.025$. The result of sensitivity analysis is quite accurate.

In Case 1, LCDLs match the UCDL profile as line flows remain below capacity limits. Because constraints are not binding, flexibility is delivered across the network without restriction. Consequently, abundant capacity ensures that DR customers at all locations share the same adjustment responsibility, resulting in uniform signals. In Case 2, LCDL1 is analogous to wind power because strict capacities of lines 1-3 and 2-3 hinder flexibility delivery from node 1 to 3, making node 1 customers bear wind consumption responsibility. During 13-17h, LCDL2 matches solar power while others match wind. As line 2-3 reaches its limit, this capacity limitation forces node 2 to consume local solar energy and hinders contributions from nodes 1 and 3. In Case 3, LCDL1 resembles solar power because node 1 is only connected to node 2 and flow limits impede flexibility delivery to node 3. Consequently, Node 1 shoulders local solar consumption. LCDL1 is lower than LCDL2 during 9-17h because line 1-2 capacity limits transmission from node 2, preventing node 1 from increasing consumption to accommodate more solar. In Case 4, disconnecting line 2-3 and other flow limits hinder flexibility between nodes 2 and 3, aligning LCDL2 and LCDL3 with local RE generation. LCDL1 reflects shared responsibility for both. Notably, line 1-2's binding limit during 14-16h increases similarity to wind, while line 1-3 capacity shortages during 1-8h and 19-24h cause mismatches.

These cases reveal that while abundant capacity allows for global sharing of load adjustment flexibility, line congestion necessitates the localization of balancing responsibilities through diverging targets. Furthermore, the established sensitivity explicitly characterizes how line capacity constraints shape these targets through a rigorous mathematical mapping.

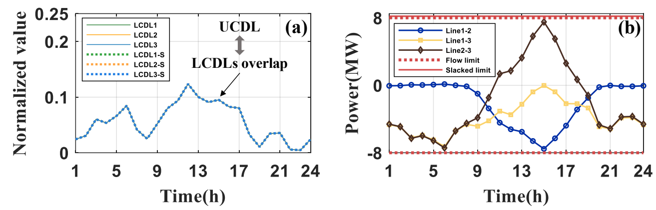

Fig. 3 Case 1. (a) LCDLs. (b) Line flow.

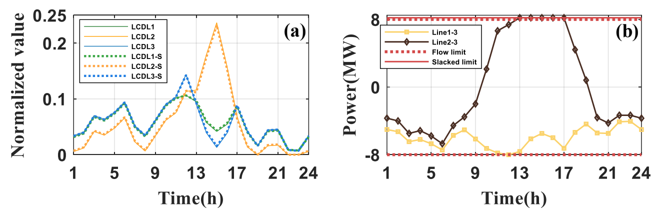

Fig. 4 Case 2 (a) LCDLs. (b) Line flow.

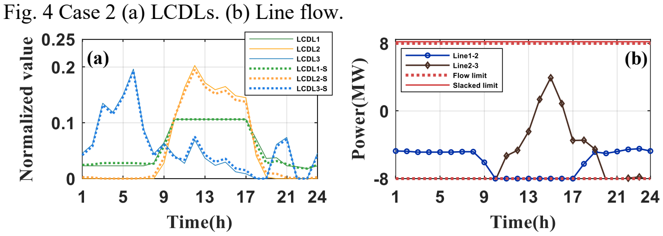

Fig. 5 Case 3 (a) LCDLs. (b) Line flow.

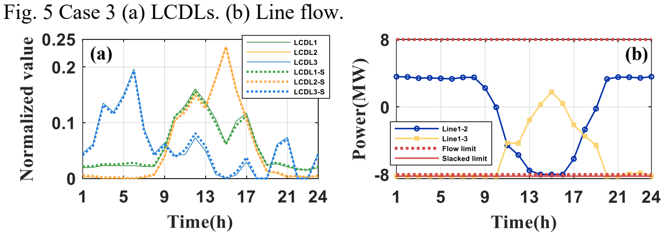

Fig. 6 Case 4 (a) LCDLs. (b) Line flow.

C. *Performance on Accommodating RE*

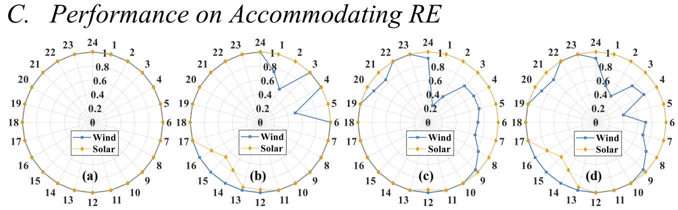

Fig. 7 Accommodation rate of renewable energy. (a)-(d): Case 1-4.

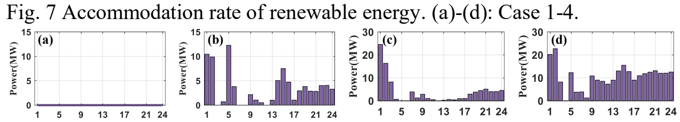

Fig. 8 Total output of virtual generators. (a)-(d): Case 1-4.

979-8-3315-8138-1

RE accommodation rates, defined as the ratio of actual to maximum power, are compared under UCDL and LCDL guidance, assuming ideal adherence to each target signal. Fig. 7 depicts the RE accommodation under UCDL; notably, the accommodation rates under LCDL guidance remain at 100% for all cases. We assume a virtual generator with sufficient capacity is situated at each node to ensure supply-demand equilibrium. Within this framework, these virtual generators provide the necessary output to satisfy the power balance constraints across all time intervals, shown in Fig. 8.

In Case 1, non-binding capacities ensure full RE accommodation. Tracking UCDL yields identical performance to LCDL because abundant capacity leads to target uniformity, as shown in Fig. 3(a). However, in Cases 2, 3, and 4, significant RE curtailment occurs due to limited line capacity. In Case 2 (14 to 16h), solar curtailment arises because UCDL is considerably lower than LCDL2 during high solar output. Consequently, UCDL fails to guide node 2 customers to increase consumption to accommodate local solar energy. Concurrently, network constraints prevent delivering flexibility from other nodes to node 2, resulting in the observed solar curtailment. Similarly, Cases 3 and 4 exhibit wind accommodation rates below unity during 1 to 8h. First, UCDL is lower than LCDL3, failing to guide node 3 customers to increase consumption for local wind absorption. Second, line capacity shortages hinder flexibility delivery from other nodes, preventing their contribution to wind absorption.

These results indicate that UCDL's global guidance fails during congestion because it ignores spatial bottlenecks, leading to RE curtailment. In contrast, the proposed LCDL-guided DR ensures complete RE accommodation.

D. Scalability analysis

The test results for the modified IEEE 30 bus system are illustrated in Fig. 9. According to Fig. 9c, Line 21 is congested during noon periods. When increasing this capacity by 0.1 MW, the resulting LCDL variations in Fig. 9b align precisely with the sensitivity distribution in Fig. 9d regarding both magnitude and direction. For instance, the LCDL changes at node 10 perfectly match the sensitivity coefficients across all time intervals. Quantitatively, the observed variations equal the product of the analytical sensitivity and the capacity increment (0.1MW). These results demonstrate the accuracy and scalability of the proposed sensitivity calculation method in larger networks.

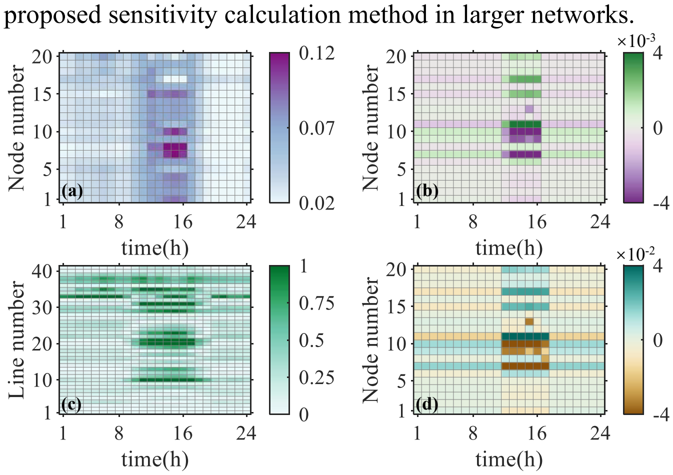

Fig. 9 Performance on the modified IEEE 30 bus system.
(a) LCDL of load nodes. (b) LCDL variations for 0.1 MW increase of Line 21 capacity. (c) Line loading rates. (d) Sensitivity of LCDL to Line 21 capacity.

Regarding computational efficiency, matrix $\boldsymbol{N}$ exhibits a block symmetric structure that facilitates faster SVD techniques through symmetry-preserving row transformations. Numerical tests show that the computational burden primarily scales with the number of congested branches rather than the total system size. For the modified IEEE 30-bus system with approximately 10 congested lines, the pseudo-inverse calculation in (23) requires only 0.62s, demonstrating high tractability for near real-time applications. While the current approach is sufficient for typical systems, future research will explore redundant constraint removal and network partitioning to further enhance scalability for massive power grids.

IV. Conclusion

This paper derives the analytical sensitivity of LCDL variation with respect to line capacity variation, establishing an explicit mapping between DR target formation and network constraints. This sensitivity elucidates how line capacity shapes LCDL profiles and quantifies the marginal contribution of locational DR targets to congestion mitigation on specific lines. Case studies validate the theoretical derivations and scalability. LCDLs converge to a uniform profile under non-binding constraints, while diverging toward local RE profiles when congestion occurs, outperforming CDL in RE accommodation.

Future work will develop incentive mechanisms to manage consumer uncertainty while further characterizing LCDL sensitivity to renewable variations for rapid intraday updates. While DC power flow reveals fundamental capacity-target mappings, we will also integrate AC constraints to address nonlinear factors in distribution-level LCDL decomposition.

References

[1] S. Chen, H. Mi, J. Ping *et al.*, "A blockchain consensus mechanism that uses Proof of Solution to optimize energy dispatch and trading," *Nature Energy*, vol. 7, no. 6, pp. 495-502, Jun. 2022.

[2] Y. Meng, S. Fan, X. Zheng *et al.*, "Optimal operation of virtual power plant considering power-to-hydrogen systems," in *2022 IEEE Power & Energy Society General Meeting*, Denver, CO, USA, Jul. 2022, pp. 1-5.

[3] International Energy Agency. World energy outlook 2022. [Online]. Available: https://www.iea.org/reports/world-energy-outlook-2022.

[4] X. Chen, Y. Li, J. Shimada *et al.*, "Online learning and distributed control for residential demand response," *IEEE Transactions on Smart Grid*, vol. 12, no. 6, pp. 4843-4853, Jun. 2021.

[5] C. Ziras, C. Heinrich, H. W. Bindner, "Why baselines are not suited for local flexibility markets," *Renewable and Sustainable Energy Reviews*, vol. 135, pp. 110357, Jan. 2021.

[6] S. Fan, Z. Li, L. Yang *et al.*: "Customer directrix load-based large-scale demand response for integrating renewable energy sources," *Electric Power Systems Research*, vol. 181, pp. 106175, Apr. 2020.

[7] Y. Meng, S. Xu, J. Hong *et al.*, "Optimal strategy for customer directrix load based demand response considering comfort and preference of customers," in *2022 IEEE PES Innovative Smart Grid Technologies-Asia (ISGT Asia)*, Singapore, Singapore, Nov. 2022, pp. 585-589.

[8] Y. Zhang, Y. Meng, S. Fan *et al.*, "Multi-time scale customer directrix load-based demand response under renewable energy and customer uncertainties," Applied Energy, Vol.383,2025, Art. no.125334.

[9] H. Ye, Z. Li, "Deliverable robust ramping products in real-time markets," *IEEE Transactions on Power Systems*, vol. 33, no. 1, pp. 5-18, Mar 2017.

[10] T. Cheng, Z. Tan and H. Zhong, "Exploiting flexibility of integrated demand response to alleviate power flow violation during line tripping contingency," *Journal of Modern Power Systems and Clean Energy*, vol. 11, no. 6, pp. 1971-1981, November 2023.

[11] Y. Meng, S. Fan, Y. Shen *et al.*, "Transmission and distribution network-constrained large-scale demand response based on locational customer directrix load for accommodating renewable energy," Applied Energy, vol.350, 2023, Art.no.121681.

[12] A. J. Conejo, E. Castillo, R. Minguez, and F. Milano, "Locational marginal price sensitivities," IEEE Trans. Power Syst., vol. 20, no. 4, pp. 2026–2033, Nov. 2005.

979-8-3315-8138-1